Micro membrane absorber with deep-permeation nano structure assembled by flowing synthesis

Boya Qiu, Senqing Fan*, Yu Chen, Jiaojiao Chen, Yilin Wang, Yinan Wang, Jingyun Liu, Zeyi Xiao

School of Chemical Engineering, Sichuan University, 610065, Chengdu, China

Abstract: A micro membrane adsorber with deep-permeation nano structure (DPNS) has been successfully fabricated by flowing synthesis. The nanoparticles are *in situ* assembled in membrane pores and immobilized in each membrane pores along the direction of membrane thickness. The nanoparticles with a lower size and thinner size distribution can be achieved owing to the confined space effect of the membrane pores. As a concept-of-proof, the nano ZIF-8 and ZIF-67 are fabricated in porous membrane pores for Methyl orange (MO) and Rhodamine B (RhB) adsorption. The adsorption rate is increased significantly owing to the enhanced contact and mass transfer in the confined space. The adsorption capacity for the RhB is also increased, since the size of the nanoparticles assembled in membrane pores is smaller with more active sites exposed. This micro membrane adsorber with DPNS has good reusability, and can provide a promising prospect for industrial application.

Key words: metal-organic frameworks; micro membrane adsorber; flowing synthesis; deep-permeated nanocomposite structure

1 Introduction

* **Corresponding Author**

Email address: fansenqing86@scu.edu.cn, Tel/Fax number: 86-028-85401057

Postal address: Sichuan University, No. 24 South Section 1, Yihuan Road, 610065 Chengdu, China

Nanomaterials have captured widespread interest in terms of adsorption over the past decades[1,2]. However, it would be hard for the nanoparticles to be applied for industry directly, since the separation and recycle of nanoparticles is difficult[3-5]. The shaping of nanoparticles as a device or an equipment is a crucial requirement for industrial applications[6-9]. Palletization by high pressure or binders are commonly used in the shaping of nano powders. However, material efficiency would be significantly decreased after the nanoparticles are scaled up or shaped by these two methods[10]. Porous membrane with tortuous pore structure and uniform pore size distribution would be a good alternative for nanoparticles immobilization[11]. Assembly of nanoparticles into the pores of the porous membrane would disperse the nanoparticles with enhanced contact and mass transfer achieved[12-14]. The tortuous pore structure could improve the immobilization stability of the nanoparticles with membrane[15]. The uniformly dispersed pores could prevent the aggregation of the nanoparticles beyond the membrane pore scale, which can enhance the contact between the nanoparticles and the adsorbate. In addition, during the adsorption process, mass transfer can be enhanced in the confined space of the membrane pores, which could weaken the concentration polarization with higher adsorption rate. Compared with the nanoparticles immobilized on the membrane surface, the thickness of the boundary layer in membrane pores can also be reduced by several orders of magnitude. Therefore, higher apparent adsorption rate can be expected in the micro membrane adsorber.

In order to obtain higher loading capacity and stability, the whole inner surface of the porous membrane along the thickness direction should be effectively utilized for the immobilization of the nanoparticles[16]. That means a deep-permeation nano structure (DPNS) should be realized in the membrane absorber. *In situ* assembly of nanoparticles in membrane pores by flowing synthesis is a feasible method for the expected DPNS[17-19]. During the flowing synthesis, the flowing of precursor solution in the membrane pores by external forces

can overcome the surface tension of the precursor solution, so that the precursor solution can be filled in each membrane pore along the whole thickness direction of the membrane[20-22]. It can avoid the possibility that nanoparticles cannot be immobilized in some membrane pores. Besides, more heterogeneous nucleation sites in the pores of membrane can be obtained, since the specific surface area is high. In this case, more nanoparticles with smaller size would be achieved.

As a concept-of-proof, herein, we fabricated a micro adsorber with nano ZIF-8 and ZIF-67 assembled in Polyethersulfone (PES) membrane pores by flowing synthesis. The adsorption performances are tested with Methyl orange (MO) and Rhodamine B (RhB) being probes. This micro membrane adsorber with DPNS can provide a promising prospect for industrial application due to its shaped structure, improved adsorption rate, and high reusability.

2 Materials and methods

2.1 Membranes and materials

The Polyethersulfone (PES) porous membrane has an average pore size of 0.45 μm, porosity of 0.7 and thickness of 100-150 μm purcharsed from Chuangwei Filter Materials Company. Cobalt nitrate hexahydrate ($Co(NO_3)_2{\cdot}6(H_2O)$), Methyl Orange (MO), Rhodamine B (RhB), and ethanol are purchased from Kelong Chemical Company. The 2-methylimidazole (2-mIm, $C_4H_6N_2$), and Triethylamine (TEA) is purchased from Aladdin. All the reagents are of analytical grade and are used as received without further modification.

2.2 Assembly of micro membrane adsorber

The schematic diagram of assembly of the micro membrane adsorber is described in **Figure 1**. Taking ZIF-67 micro membrane adsorber as an example. Before synthesis processes, PES membranes are cleaned with DI water. After the membranes are dried and weighed, a typical cycle of the assembly process is as follows: firstly, the $Co(NO_3)_2{\cdot}6(H_2O)$

(2.46 mmol) is dissolved in 50 mL DI water, and the solution flows across PES membranes under pressure by compressed nitrogen, in order to make the solution permeate into membrane pores deeply and slowly. Secondly, after the permeating process lasts for about 20 min, the membranes are taken out and dried in the vacuum oven at 60°C for 30 min. Thirdly, the mixed solution of 2-mIm (19.75 mmol) and TEA (19.76 mmol) in 50 mL DI water is stirred until dissolved, and the solution flows across the membrane under pressure, therefore nano ZIF-67 is synthesized in membrane pores. At last, after the permeating process lasts for about 20 min, the membranes are taken out and dried in the vacuum oven at 60°C for 30 min, then washed with DI water under ultrasonic to remove the nanoparticles immobilized on the surface of PES membranes. The membranes are weighted after every cycle in order to calculate the loading of ZIF-67. Repeat the synthesis cycle, and the micro adsorber with different ZIF-67 loading ratio could be obtained. The visual image of the membrane during the assembly process of the ZIF-67 and ZIF-8 micro membrane adsorbers are illustrated in **Figure S1**.

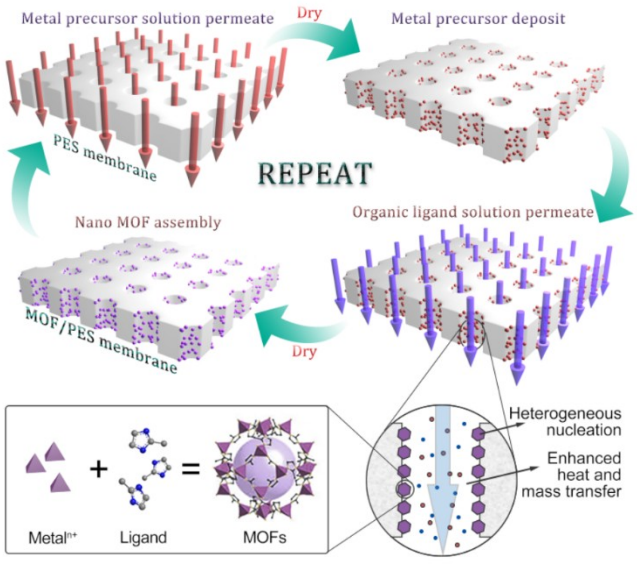

Figure 1. Schematic diagram of fabricating micro membrane adsorber with DPNS.

2.3 Adsorption experiments

Continuous adsorption and batch adsorption mode are applied respectively as can be seen in **Figure 2**. The process of the continuous adsorption by micro membrane adsorber is as follows: The dye solution is prepared as the reactant solution in advance. The micro membrane adsorber is fixed in the membrane module. Then, the solution is pumped to flow through the membrane pores compulsively by a peristaltic pump. The flowrate of the solution can be adjusted by the peristaltic pump.

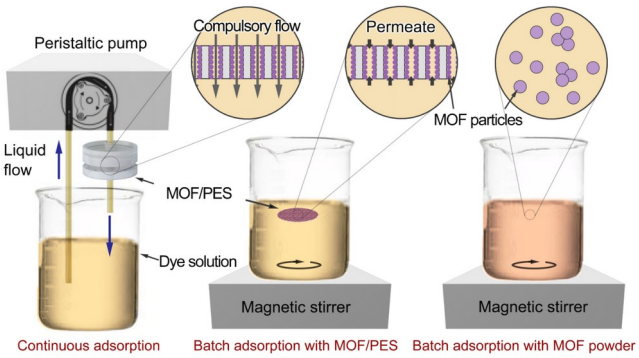

Figure 2. Diagram of adsorption process using the micro membrane adsorber and the MOF powders through batch adsorption and continuous adsorption

During the batch adsorption process, the micro membrane adsorber and the MOF powders are soaked in the reaction solution and the solution is stirred with a magnetic stirrer. The reaction condition including the concentration and the amount of the dye solution, temperature, pH, the amount of the MOFs, and the reaction time are all kept the same as those in continuous mode.

2.4 Analysis methods

The morphologies of the materials are detected by a field emission scanning electron microscopy (FESEM), and are acquired using a JEOL JSM-7500f scanning electron microscope at an accelerating voltage of 15 kV. The distribution of elements are obtained with the energy-dispersive spectrometers (EDS) (HITACHI SU3500 scanning electron microscopy (SEM)). The specimens are obtained by saturating the membranes into ethanol and then breaking them in liquid nitrogen. The specimens are coated with 10 nm of Au using

a HITACHI MCIOOO ion sputter before characterization. The X-ray diffraction (XRD) patterns are recorded using an EMPYREAN diffractometer with a CuKα radiation source to analyze the crystal structures. The X-ray photoelectron spectroscopy (XPS) data are collected on an ESCALab220i-XL electron spectrometer using a 300 W AlKα radiation. The specific surface area and the pore volume of the materials are obtained from Quantachrome Instruments version 11.02. The Brunauer-Emmett-Teller (BET) surface area is calculated from the multipoint BET data using the standard BET equation. The range of relative pressure is 0.07-0.3. The total pore volume is evaluated by converting the adsorption amount at P/P_0=0.99 to a volume of liquid adsorbate. The micropore volume is obtained using the t-plot method of Lippens and de Boer to the adsorption data.

All experiments are performed in duplicate. Solution pH is adjusted by dilute HCl or dilute NaOH solution. The concentration of MO and RhB is measured with a UV-vis spectrophotometer at 464 and 555 nm, respectively. The adsorption capacity is calculated based on **Eq. (1)**:

$$q = \frac{\left(C_0 - C_e\right)V}{m_{MOF}} \tag{1}$$

where q is the adsorption capacity (mg g^{-1}), C_0 is the initial concentration of the dye in solution (mg L^{-1}), C_t is the concentration of the dye at time t (mg L^{-1}), m is the mass of the adsorbent (g), and V is the volume of the solution (L).

During the adsorption experiment adsorbed by the micro membrane adsorber, the mass of the adsorbent (m_{MOFs}) is calculated as follows:

$$m_{MOF} = m_i - m_0 \tag{2}$$

where m_i is the mass of the micro membrane adsorber (g), m_0 is the mass of pristine PES membranes (g).

The loading of MOFs (ϕ_i) can be calculated as follows:

$$\phi_t = \frac{(m_t - m_0)}{m_0} \tag{3}$$

For the study of adsorption kinetic, the pseudo-first-order kinetic model, pseudo-second-order kinetic model and inter-particle diffusion model are used to fit the experimental data, which can be seen as follows:

$$\ln(q_e - q_t) = \ln q_e - k_1 t \tag{4}$$

$$\frac{t}{q_t} = \frac{1}{k_2 q_e^2} + \frac{t}{q_e} \tag{5}$$

$$q_t = k_d t^{0.5} + C \tag{6}$$

where t is the adsorption time (h), q_t (mg g^{-1}) is the adsorption capacity at time t, and q_e (mg g^{-1}) is the adsorption capacity when the adsorption equilibrium is obtained. k_1 (h^{-1}), k_2 (g mg^{-1} h^{-1}), k_d (g mg^{-1} $h^{-0.5}$) are the adsorption rate constant of the pseudo-first-order kinetic, pseudo-second-order kinetic, and inter-particle diffusion models, respectively.

The calculation of BET surface area of the MOF powders inside the PES membrane pores is described in our previous work[17].

2.5 Theory

The adsorption by a particle is illustrated in **Figure S2**. The adsorbate needs to transfer across an outside boundary layer before contacting with the particle and the diffusion rate can be described as follows:

$$R_d = \frac{D}{\delta}(C - C_i) \tag{7}$$

where R_d represents the diffusion rate, D represents the diffusion coefficient, and δ is the thickness of the boundary layer around the nanoparticles. C and C_i are the concentration of the adsorbate in the bulk solution and at the interface of the liquid and the surface of the nanoparticles, respectively.

The adsorbate being adsorbed in the nanoparticles can also be calculated as Eq. (8):

$$R_{app}=C_i \cdot k_i \tag{8}$$

where the R_{app} is the adsorption rate, and the k_i is the intrinsic adsorption rate constant.

The adsorption rate is equal to the diffusion rate under the condition of steady adsorption, which can be described as follows:

$$R_d = R_{app} \tag{9}$$

Combining Eq.(7)~Eq.(9), the adsorption rate by a particle can be described as follows:

$$R_{app} = \frac{C}{\frac{\delta}{D}+\frac{1}{k_i}} \tag{10}$$

3 Results and discussion

3.1 Characterization of micro membrane adsorber

In order to illustrate the successful assembly of MOFs in PES membranes and successful construction of the micro membrane adsorber, the as-synthesized ZIF-67 and ZIF-8 micro membrane adsorbers are thoroughly characterized as illustrated in **Figure 3**. According to the X-ray diffraction (XRD) data, they both exhibited strong diffraction patterns, which are consistent with the corresponding simulated ZIF-67 and ZIF-8 as illustrated in **Figure 3(A)**. XPS analysis is also carried out as can be seen in **Figure 3(B-D)**. Only peaks of C, N, and O can be found on the wide-scan XPS spectrum of the pristine PES membrane. After the assembly of ZIF-67 and ZIF-8, the peak of Co (392-410 eV) appears, and the peak of C (392-410 eV) and N (525-545 eV) increased. Meanwhile, the C-N bond in the micro membrane adsorbers are increased, which can be attributed to the 2-Im^-. In addition, both Zn and Co are bivalent. Furthermore, the bonds including the C-N bond (995 cm^{-1}) and imidazole ring (1350-1500 cm^{-1} and 500-800 cm^{-1}) in 2-Im^- can be seen in the FTIR spectrum in **Figure 3(E)**. Besides, the Co-N bond and Zn-N bond appear at 424 cm^{-1} and 420 cm^{-1} respectively

(**Figure 3(F)**). They all demonstrate the successful assembly of the micro membrane adsorber.

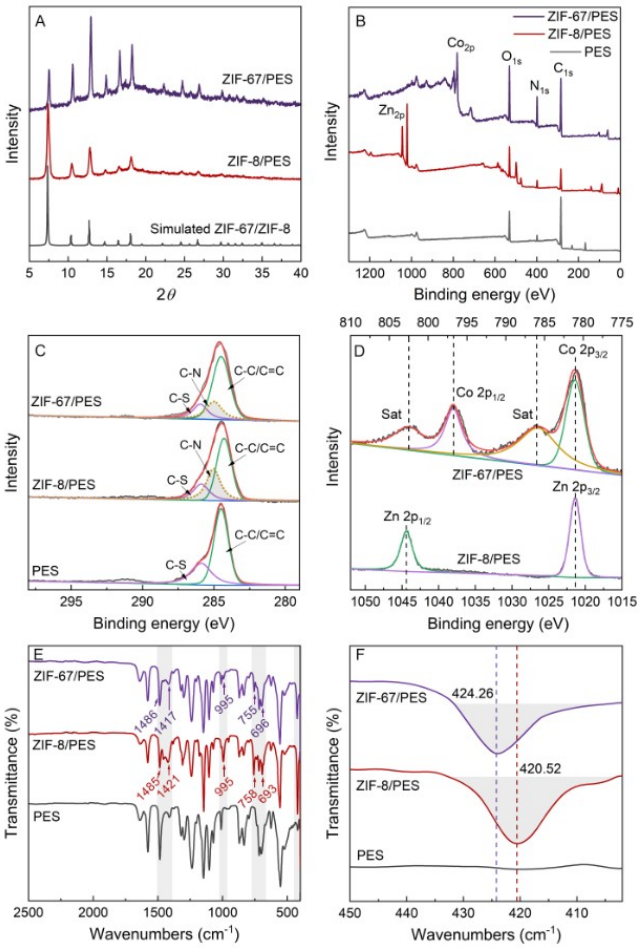

Figure 3. Characterization of ZIF-67 and ZIF-8 micro membrane adsorber (A: XRD; B: XPS; C: high-resolution spectrum of C 1s; D: high-resolution spectrum of Co 2p and Zn 2p; E-F: FTIR characterization)

Table 1. BET measurements of the pristine PES membrane and the ZIF-67 and ZIF-8 micro membrane adsorber

Membrane	BET surface area (m^2 g^{-1})	Pore volume (cm^3 g^{-1})
PES	0.82	0.0003
ZIF-67/PES	270.58	0.385
ZIF-67 in ZIF-67/PES (calculated)	870.04	0.558

ZIF-8/PES	324.86	0.1149
ZIF-8 in ZIF-8/PES (calculated)	1250.69	0.4423

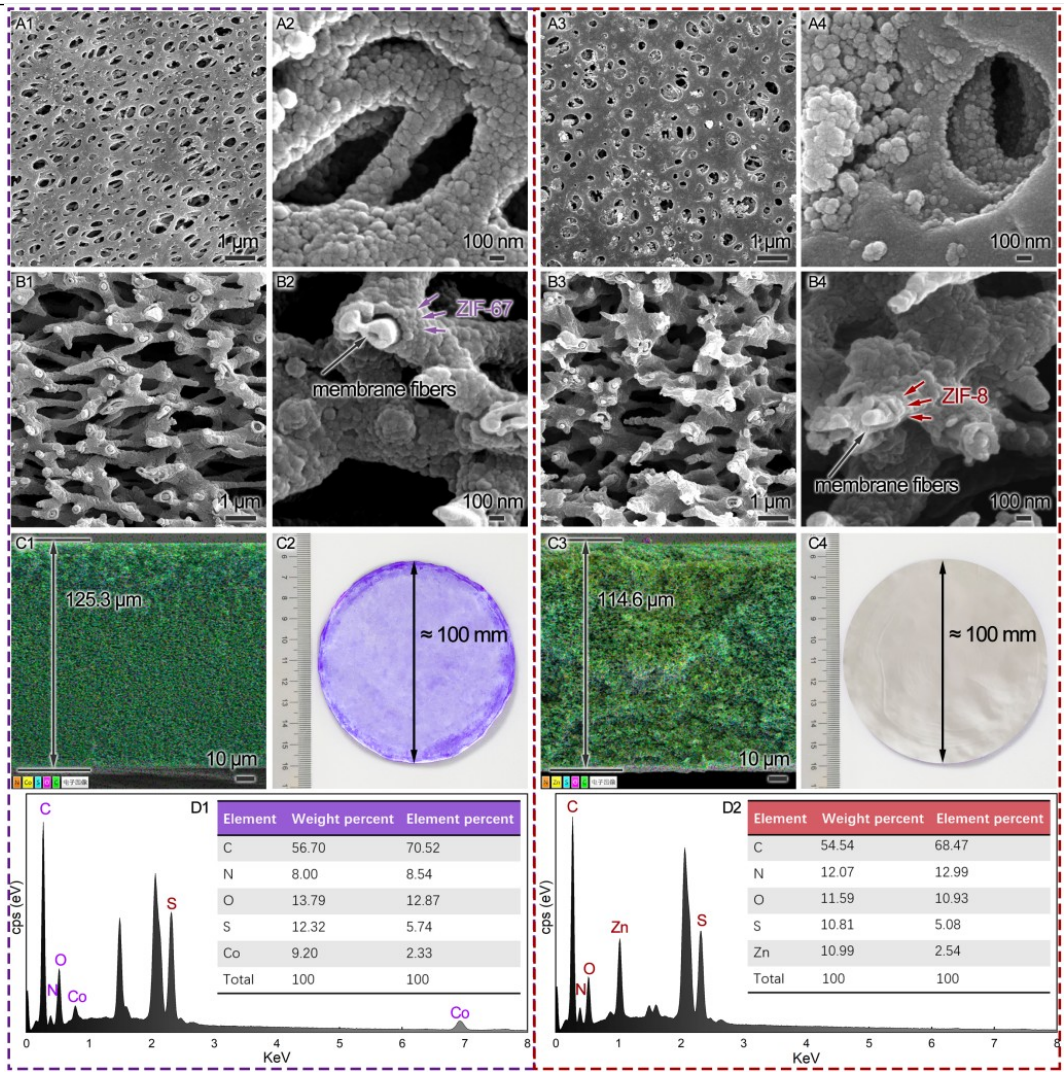

Figure 4. the morphology and element distribution of the ZIF-67 (A) and ZIF-8 (B) micro membrane adsorbers (A1-A4: FESEM image of the membrane surface; B1-B4: FESEM image of the membrane cross-sectional surface; C1, C3: EDS mapping; C2, C4: The optical image of membrane; D1-D2: EDS analysis)

Besides, according to TGA analysis (**Figure S3**), the remaining mass of the micro membrane adsorber is higher than that of the pristine PES membrane, after the temperature is increased to 1000°C. In addition, after the ZIF-67 assembly, the BET surface area is also

increased from 0.82 $m^2 g^{-1}$ to 270.58 $m^2 g^{-1}$ as illustrated in **Table 1**, the pore volume of the composite structure also increased by three orders of magnitude after ZIF-67 assembled. It can be calculated that the BET surface area and pore volume of the ZIF-67 synthesized in PES membrane is 870.04 $m^2 g^{-1}$ and 0.558 respectively, which is close to the literature reported[23].

In order to further demonstrate the distribution and morphological characteristics of ZIF-67 and ZIF-8 in the PES membrane, the cross-sectional FESEM analysis of the micro membrane adsorber is carried out. In order to stabilize the immobilization of nanoparticles inside the membrane pores, both ZIF-8 and ZIF-67 micro membrane adsorber are ultrasonic washed to remove the unstable nanoparticles. It has been observed from **Figure 4(A1-A4)** that the nanoparticles on the surface of the membrane while those inside the pores can be removed. From the pores exposed on the surface of the membrane, nanoparticles are immobilized on the membrane fibers. The immobilization of ZIF-67 and ZIF-8 on the PES membrane fibers can also be seen from the cross-sectional surface of the PES membrane (**Figure 4(B1-B4)**). The membrane pores are still maintained, as the size of the nanoparticles is relatively low. Therefore, the membrane can still provide micro-channels for the flow of the fluid. The ZIF-67 and ZIF-8 nanoparticles can also distribute evenly along the whole membrane thickness, owing to the uniform distribution of the membrane pores. The even distribution of the nanoparticles in the membrane can be demonstrated by the EDS mapping as illustrated in **Figure 4(C1, C3)**. Elements including C, N, O, S, Co, and Zn all show even distribution throughout the whole membrane thickness (**Figure S4**). In addition, the colors of the micro membrane adsorbers are also even, demonstrating the even distribution of ZIF-67 and ZIF-8 nanoparticles along the membrane surface direction (**Figure 4(C2, C4)**). Therefore, taking advantage of the evenness of the porous membrane as well as the flowing-

synthesis method, the ZIF-67 and ZIF-8 can be immobilized in the PES membrane evenly and thoroughly, which would be a benefit for the utilization of those nanoparticles.

The size distribution of nanoparticles synthesized in the micro-channels of the PES membrane is further illustrated in **Figure 5**. The morphology of ZIF-8 and ZIF-67 is compared with the nanoparticle powders synthesized by the batch method. Both ZIF-8 and ZIF-67 immobilized in the membrane pores are smaller in size than those powders synthesized by the batch method under the same condition. Specifically, the size of ZIF-67 is decreased from 190 nm to 48 nm on average when the batch method is changed to the flowing synthesis method, while the size of ZIF-8 is decreased from 125 nm to 37 nm. Each average size is reduced by 70-80 %. This could be due to the special reaction condition due to the nanopore structure of the PES membrane.

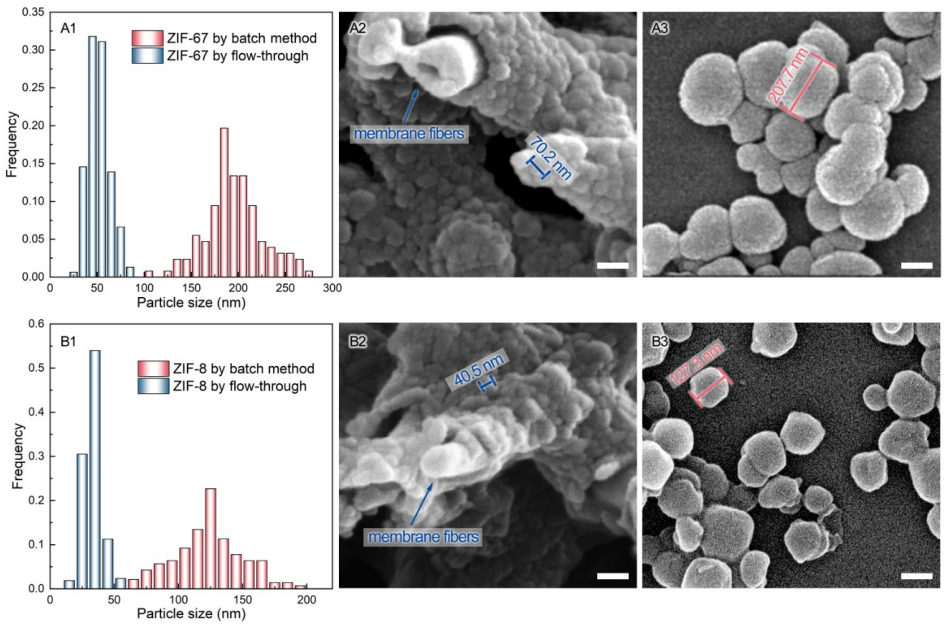

Figure 5. Size distributions (A1, B1) and morphologies of ZIF-8 and ZIF-67 in PES membrane pores through flowing synthesis (A2, B2) and through batch method (A3, B3)

Firstly, nanoparticles are preferentially nuclear and grow on the reactor wall, due to the heterogeneous nucleation effect as illustrated in **Figure 1**. When the nanoparticles are synthesized in the membrane pores, the large surface area of the inner membrane can provide

a large platform for the heterogeneous nucleation of the MOFs. Therefore, most of the nanoparticles would grow on the membrane fibers, with relatively even particle size. Secondly, due to the confinement of the micro-channels of the PES membrane, when the precursor solution flows through the membrane pores, the boundary layer can be no larger than the pore size, and it can be significantly thinned. In addition, the complex structure of the membrane pores can easily disturb the fluid flow, thereby increasing the complexity of the flow condition, and further reduce the boundary layer and promote the heat and mass transfer of the fluid. Furthermore, the metal precursor and the organic linkers can be mixed in millisecond, due to the short mass transfer path in the confined space of the membrane pores. s. The fresh precursor molecules can also be replenished due to the continuous flow of the procurer solution, therefore provide a more homogeneous environment for the synthesis of ZIF-8 and ZIF-67. As a result, the size of the nanoparticles synthesized in the membrane pores will be evener, with a thinner size distribution. In addition, the density of the nucleation of the ZIF-8 and ZIF-67 can be large due to the large surface area in the membrane pores. Therefore, the growth of the nanoparticles can be relatively low under the same reaction, thus the nanoparticles synthesized in the membrane pores can be smaller.

Based on the discussion, ZIF-67 and ZIF-8 can be synthesized in the PES membrane pores by the flow synthesis method, with the micro membrane adsorber assembled. The nanoparticles immobilized in the membrane pores have a lower size and thinner size distribution than those synthesized by the batch method.

3.2 Improved adsorption performance

In order to test the adsorption performance of the ZIF-67 and ZIF-8 micro membrane adsorber, MO and RhB are taking as two probes. The mechanisms of the micro membrane adsorber have been illustrated in **Figure S5** and **Figure S6**. The adsorption performance of the micro membrane adsorber is illustrated in **Figure 6(A-D)**, as well as the result of the

kinetics fitting. The specific details of the kinetic models are illustrated in **Table S1**. This shows that, compared with the pseudo-first-order kinetic model, the pseudo-second-order kinetic model is more suitable for the adsorption process of MO and RhB on ZIF-8 and ZIF-67. It is proved that the adsorption process is mainly chemical adsorption. According to the pseudo-second-order kinetic model, the micro membrane adsorber has higher adsorption than the corresponding powders. For example, when the ZIF-8 powders are used for the adsorption of MO, the adsorption rate constant is 0.033 g mg^{-1} h^{-1}. In comparison, the adsorption rate constant of the ZIF-67 micro membrane adsorber for MO adsorption is increased by over 3 times to 0.109 g mg^{-1} h^{-1}, with the continuous adsorption mode applied. Similar rules can also be speculated during the adsorption of MO by ZIF-67, as well as the adsorption of RhB and MO by ZIF-8. This implies that the micro membrane adsorber can promote the absorption rate during the continuous adsorption process. This could be due to the enhanced mass and heat transfer. The mass and heat transfer conditions are relatively poor when the MOF powders are used as adsorbate with batch mode applied, due to the relatively thick boundary layer at the surface of the MOF powders, as well as the high aggregation tendency of nano MOFs. Furthermore, both the dispersion of the nanoparticles and the flow condition will further deteriorate if the volume of the reactor increases, so it is difficult to expand its industrial application.

On the contrary, the micro membrane adsorber we developed can provide micro-channels for the continuous flow of the adsorbent solution. According to the adsorption mathematical model (**Eq. (10)**), it can be deduced that the apparent adsorption rate can be increased with the decrease of the thickness of the boundary layer. The thickness of the boundary layer at the surface of the nanoparticles immobilized in the membrane pores can be reduced to sub-micrometer, when the absorbent solution flows across the micro-scaled membrane pores. Therefore, the thickness of the boundary layer in the membrane pores can

be reduced by several orders of magnitude, compared with the nanoparticles immobilized on the membrane surface. As a result, the outer diffusion would be enhanced. In addition, as the nanoparticles are immobilized in the membrane pores with high dispersity, they can be exposed to the adsorbent solution effectively. The immobilization can reduce the surface energy of the nanoparticles, thereby preventing the aggregate of the MOF particles during the adsorption process, meanwhile, the confined space effect of the nanopores would also preventing the aggregation of the nanoparticles beyond the membrane pore scale. Therefore, the contact of the nanoparticles and the adsorbate could be enhanced. As a result, the adsorption rate can be improved due to the structure of the micro membrane adsorber and the continuous reaction mode. Furthermore, the micro membrane adsorber can be easily scaled-up by increasing the membrane area, while the enhanced mass transfer could be maintained during the scale-up process. Therefore, the use of the micro membrane adsorbers not only can improve the adsorption rate but also are an effective way for their large-scale application in industry.

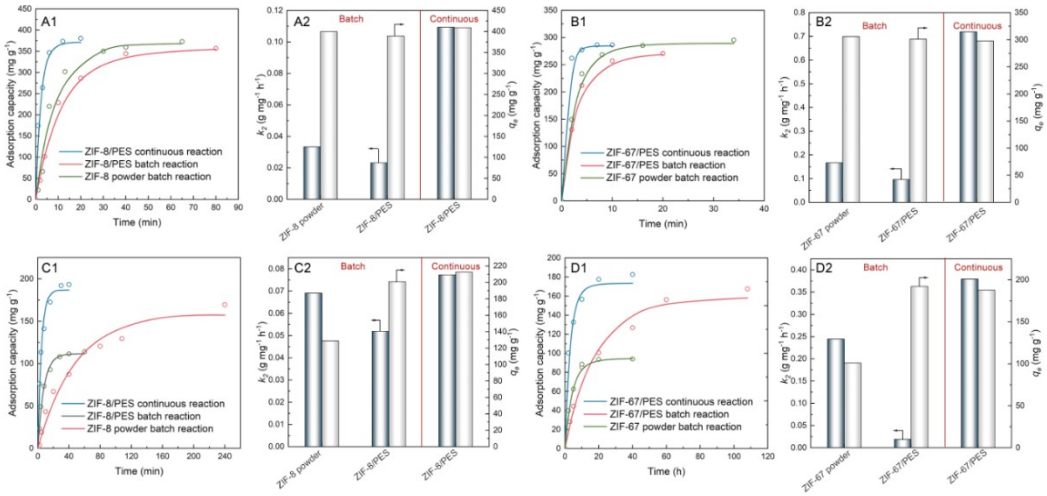

Figure 6. Adsorption property of ZIF-8 and ZIF-67 micro membrane adsorbers (A1-A2, B1-B2: the adsorption curves and the adsorption kinetic models of MOF powders and MOF micro-adsorber for MO adsorption; C1-C2, D1-D2: the adsorption curves and the adsorption kinetic models of MOF powders and MOF micro-adsorber for RhB adsorption; concentration

and volume of MO and RhB solution: 40 mg L^{-1}, 25 mL, mass of the ZIF-8 and ZIF-67 powders: 0.02 g; room temperature)

The flowrate of the dye solution across the membrane pores is one of the primary factors affecting the mass transfer and the thickness of the boundary layer around the adsorbate. Therefore, the effect of the flowrate on the adsorption behavior of the ZIF-8 and ZIF-67 micro membrane adsorbers is further illustrated, as can be seen in **Figure 7**. According to **Figure 7(A)**, when the flow rate is 10 mL min^{-1}, the adsorption rate constant of ZIF-8 micro membrane adsorber for MO adsorption is 0.098 g mg^{-1} min^{-1}. As the flowrate increases, the adsorption rate constant increases significantly. Specifically, the adsorption rate constant is increased to 0.79 mg min^{-1} by about an order of magnitude, when the flowrate is increased to 50 mL min^{-1}. The adsorption behaviors of ZIF-8 micro membrane adsorber for RhB and ZIF-67 micro membrane adsorber for MO and RhB show similar trends, as illustrated in **Figure 7(B-D).** This could be mainly due to the enhanced mass transfer rate in the membrane pores. When the flowrate is low, the mass transfer would be relatively low. In this case, the dye molecules cannot be replenished in time due to the relatively intrinsic higher adsorption rate, resulting in a thicker boundary layer around the adsorbate nanoparticles. Therefore, the concentration of the dye molecular at the surface of the adsorbate would be lower than that of the bulk solution. As a result, the adsorption rate could be limited. However, if the flowrate is increased, the mass transfer would be enhanced, the boundary layer would be thinner, and fresh dye molecules could be more likely to transfer to the surface of the MOF particles. Therefore, the adsorption rate would be increased. As a result, utilizing MOF micro membrane adsorber rather than MOF powders are more likely to maximize the adsorption efficiency of the adsorbate, and facilitate the efficient use of the adsorbent in industry.

Apart from the enhanced adsorption rate, it is worth noting that the adsorption capacity for RhB by ZIF-67 and ZIF-8 can be improved, if the micro membrane adsorber is used, as

illustrated in **Figure 6(C-D),** as well as in **Figure 8(A)**. On the contrary, the adsorption capacity for the MO has no significant change (**Figure 6(A-B)**, **Figure 8(B)**). As the adsorption and rejection of the PES membrane for the MO and RhB are low (**Figure S7**). The improved adsorption capacity could be attributed to the difference between the adsorption mechanism between MO and RhB. According to the intra-particle diffusion model, a typical adsorption process for porous materials including 3 stages: outer diffusion step, inner diffusion step, and the intrinsic adsorption. The adsorption process of MO by the micro membrane adsorbers are correspondent to this mechanism and can be divided into 3 steps. However, the adsorption of the RhB can only be divided into 2 steps and the inner diffusion step is not obvious in this process. Therefore, it can be deduced that the MO can be diffused into the pores of the ZIF-67 and the ZIF-8, while the RhB cannot.

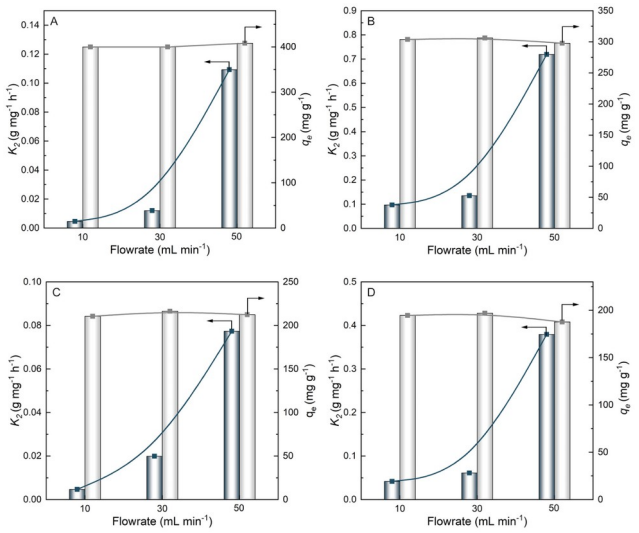

Figure 7. Effect of flowrate on the adsorption for MO and RhB by ZIF-8 and ZIF-67 micro membrane adsorber(A: ZIF-8 micro membrane adsorber for MO adsorption; B: ZIF-67 micro membrane for MO adsorption; C: ZIF-8 micro membrane adsorber for RhB adsorption; D: ZIF-67 micro membrane adsorber for RhB adsorption; concentration and volume of MO and RhB solution: 40 mg L^{-1}, 25 mL, mass of the ZIF-8 and ZIF-67 powders: 0.02 g; room temperature)

This phenomenon could be due to the different molecular size of MO and RhB. Since MO has a low molecular size ($1.31 \times 0.55 \times 0.18\ nm^3$), it can enter the inner pores of ZIF-8 (≈3.4 Å) and ZIF-67 (≈10 Å). In this case, both the adsorption site inside and outside of the nanoparticles can be utilized. However, the molecular size of RhB is relatively large ($1.59 \times 1.18 \times 0.56\ nm^3$) and cannot enter the inner pores of ZIF-8 and ZIF-67. Therefore, most of them can only be adsorbed on the surface of the nanoparticles. In this case, the MOF particles with a larger exposed outer surface would be more favorable. This phenomenon has also been reported in the previous reports[23,24]. As ZIF-67 and ZIF-8 nanoparticles in the micro membrane adsorber has a lower size, and the aggregation of the nanoparticles during the adsorption process can be prevented due to the adhesion between particles and the membrane substrate, the exposed outer surface area of the MOF could be larger than the MOF powders synthesized by the batch reaction. As a result, the novel micro membrane adsorber has a higher adsorption capacity for some relatively large molecules like RhB.

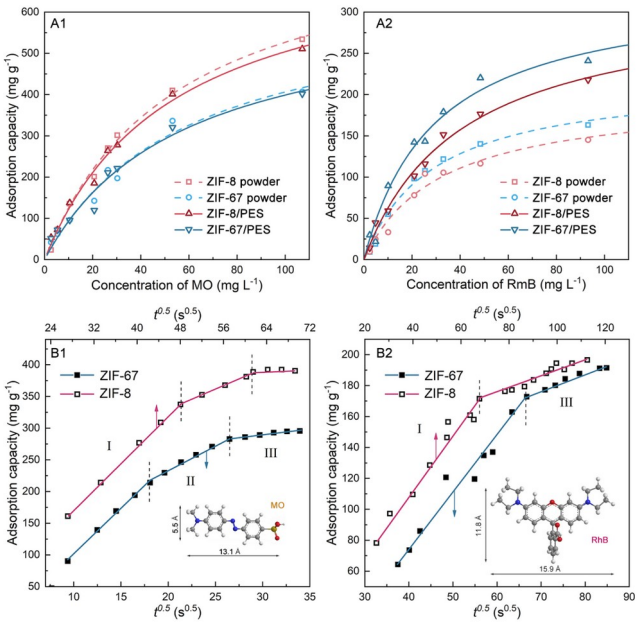

Figure 8. the adsorption isotherm curves and the intro-particle diffusion model for adsorption of MO (A1, B1) and RhB (A2, B2) onto ZIF-67 and ZIF-8 micro membrane adsorber

(concentration and volume of MO and RhB solution: 40 mg L^{-1}, 4 mL, mass of the ZIF-8 and ZIF-67 powders: 0.003 g, mass of micro membrane adsorber: 0.006 g; room temperature)

3.3 Enhanced repeatability

Immobilizing the nanoparticles inside the membrane pores can effectively enhance the stability and reusability of the material. As shown in **Figure 9**, the adsorption performance of the micro membrane adsorber is relatively stable. For example, the adsorption capacity of ZIF-67 micro membrane adsorber can only be reduced by lower than 20% after 5 repeated adsorption processes. This could be partially due to the stable immobilization of nanoparticles in membrane pores. In addition, compared with MOF powders, the reuse of the micro membrane adsorber can prevent the centrifugation process, thereby further decreasing the loss of the MOF materials. It can be implied that the energy consumption can also be reduced, due to the high stability of the micro membrane adsorbers, as well as their convenient reuse. As an exception, the ZIF-8 micro membrane adsorber has relatively low reusability, which could be due to the high interaction between ZIF-8 and MO. Therefore, the desorption of the MO from ZIF-8 would be difficult and incomplete, which leads to the reduced adsorption capacity.

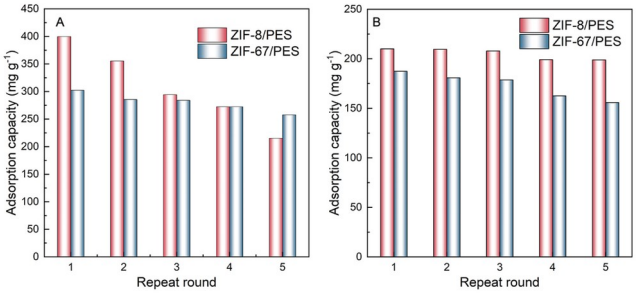

Figure 9. The reusability of the MOF micro membrane adsorber; concentration and volume of MO and RhB solution: 40 mg L^{-1}, 4 mL, mass of the ZIF-8 and ZIF-67 powders: 0.003 g, mass of micro membrane adsorber: 0.006 g; room temperature)

4 Conclusions

In summary, we have developed a micro membrane adsorber by the flowing synthesis method. The ZIF-8 and ZIF-67 nanoparticles were *in situ* synthesized and immobilized evenly in the whole inner surface of the PES porous membranes. The nanoparticles synthesized by the flow synthesis method had a lower size and a thinner size distribution than that by the batch method. The adsorption rate constant of the micro membrane adsorber for MO and RhB through the continuous mode was higher than that of the corresponding powders through batch adsorption. The adsorption capacity of the micro membrane adsorber for the RhB was also increased compared with that of the ZIF-8 and ZIF-67 powders. The micro membrane adsorber had good reusability. This structure provided a feasible choice for the industrial application of MOFs for adsorption.

Associated content

The following files are available.

Supporting information (PDF) The visual image of the membrane during the assembly process of the ZIF-67 micro membrane adsorbers (Figure S1); Schematic diagram of the adsorption process (Figure S2); TGA analysis of ZIF-67 and ZIF-8 micro membrane adsorbers (Figure S3); EDS mapping of the cross-sectional surface of the ZIF-67 and ZIF-8 micro membrane adsorbers (Figure S4); Mechanism of the adsorption of MO and RhB by micro membrane adsorber (Figure S5); Adsorption capacity of MO and RhB by ZIF-8 and ZIF-67 micro membrane adsorber under different pH value (Figure S6); Adsorption and rejection performance of the pristine PES membrane (Figure S7); The fitting results of adsorption kinetics for MO and RhB onto ZIF-8 and ZIF-67 powders and micro membrane adsorbers (Table S1)

Author contributions

Boya Qiu performs experiments, data analysis, figures plotting and manuscript writing with input from all coauthors; Senqing Fan leads the experiments design, formal analysis and

contributes to manuscript writing, and is the project administration and leads the whole project; Zeyi Xiao leads the supervision and takes part in the and discussion of the project; Other coauthors contributed equally to this work on helping experiment and analysis.

Acknowledgements

The present work was supported by the National Nature Science Foundation of China (No. 21808144) and the Fundamental Research Funds for the Central Universities (No. 20822041B4013).

Competing interests statement

Declarations of interest: none

Nomenclature

q	Adsorption capacity
C	Concentration of the adsorbate
ϕ_{MOF}	Loading ratio of the MOFs in the adsorber
m_i	Total mass of the micro membrane adsorber
m_0	Mass of the pristine PES membrane
k_1	Adsorption rate constant of the pseudo-first-order kinetic
k_2	Adsorption rate constant of the pseudo-second-order kinetic
k_d	Adsorption rate constant of the inter-particle diffusion model
S	BET surface area
x	Weight percent of MOFs or PES in micro membrane adsorber
R_d	Diffusion rate
D	Diffusion coefficient of the adsorbate
R_{app}	Adsorption rate
k_i	Intrinsic adsorption rate constant

Greek letters

ϕ Loading ratio of MOFs

δ Thickness of the boundary layer

Subscripts and superscripts

0 At the beginning of the adsorption process

t Adsorption time

e At the time when adsorption equilibrium is obtained

References

1. Li H, Eddaoudi M, O'Keeffe M, Yaghi OM. Design and synthesis of an exceptionally stable and highly porous metal-organic framework. *Nature.* 1999;402(6759):276-279.

2. Eddaoudi M, Kim J, Rosi N, et al. Systematic design of pore size and functionality in isoreticular MOFs and their application in methane storage. *Science.* 2002;295(5554):469-472.

3. Xiong S, Kong L, Zhong Z, Wang Y. Dye adsorption on zinc oxide nanoparticulates atomic-layer-deposited on polytetrafluoroethylene membranes. *AIChE Journal.* 2016;62(11):3982-3991.

4. Seto H, Yoneda T, Morii T, Hoshino Y, Miura Y, Murakami T. Membrane reactor immobilized with palladium-loaded polymer nanogel for continuous-flow Suzuki coupling reaction. *AIChE Journal.* 2015;61(2):582-589.

5. Miao J, Lu J, Jiang H, et al. Continuous and complete conversion of high concentration p-nitrophenol in a flow-through membrane reactor. *AIChE Journal.* 2019;65(9):e16692.

6. Thakkar H, Eastman S, Al-Naddaf Q, Rownaghi AA, Rezaei F. 3D-Printed Metal-Organic Framework Monoliths for Gas Adsorption Processes. *ACS Applied Materials and Interfaces.* 2017;9(41):35908-35916.

7. Peterson GW, DeCoste JB, Glover TG, Huang YG, Jasuja H, Walton KS. Effects of

pelletization pressure on the physical and chemical properties of the metal-organic frameworks Cu-3(BTC)(2) and UiO-66. *Microporous and Mesoporous Materials.* 2013;179:48-53.

8. Chen Y, Huang X, Zhang S, et al. Shaping of Metal-Organic Frameworks: From Fluid to Shaped Bodies and Robust Foams. *Journal of the American Chemical Society.* 2016;138(34):10810-10813.

9. Rezaei F, Lawson S, Hosseini H, et al. MOF-74 and UTSA-16 film growth on monolithic structures and their CO2 adsorption performance. *Chemical Engineering Journal.* 2017;313:1346-1353.

10. Silva P, Vilela SMF, Tomé JPC, Almeida Paz FA. Multifunctional metal–organic frameworks: from academia to industrial applications. *Chemical Society Reviews* 2015;44(19):6774-6803.

11. Ruan X, Xu Y, Liao X, et al. Polyethyleneimine-grafted membranes for simultaneously adsorbing heavy metal ions and rejecting suspended particles in wastewater. *AIChE Journal.* 2017;63(10):4541-4548.

12. Chen X, Wang Z, Bi S, et al. Combining catalysis and separation on a PVDF/ Ag composite membrane allows timely separation of products during reaction process. *Chemical Engineering Journal.* 2016;295:518-529.

13. Wang J, Wu Z, Li T, et al. Catalytic PVDF membrane for continuous reduction and separation of p-nitrophenol and methylene blue in emulsified oil solution. *Chemical Engineering Journal.* 2018;334:579-586.

14. Wang J, Ng CK, Cao B, Qing W, Liu F, Tang CY. Polydopamine enabled palladium loaded nanofibrous membrane and its catalytic performance for trichloroethene dechlorination. *Applied Catalysis A: General.* 2018;559:122-126.

15. Strano MS, Foley HC. Synthesis and characterization of catalytic nanoporous

carbon membranes. *AIChE Journal.* 2001;47(1):66-78.

16. Huang N, Drake H, Li J, et al. Flexible and Hierarchical Metal-Organic Framework Composites for High-Performance Catalysis. *Angewandte Chemie.* 2018;57(29):8916-8920.

17. Qiu B, Fan S, Wang Y, et al. Catalytic membrane micro-reactor with nano ZIF-8 immobilized in membrane pores for enhanced Knoevenagel reaction of Benzaldehyde and Ethyl cyanoacetate. *Chemical Engineering Journal.* 2020;400:125910.

18. Chen Y, Fan S, Qiu B, et al. Enhanced Catalytic Performance of a Membrane Microreactor by Immobilizing ZIF-8-Derived Nano-Ag via Ion Exchange. *Industrial & Engineering Chemistry Research.* 2020;59(44):19553-19563.

19. Qin Y, Jian S, Bai K, et al. Catalytic Membrane Reactor of Nano (Ag+ZIF-8)@Poly(tetrafluoroethylene) Built by Deep-Permeation Synthesis Fabrication. *Industrial & Engineering Chemistry Research.* 2020;59(21):9890-9899.

20. Li H, Jiang H, Chen R, Wang Y, Xing W. Enhanced Catalytic Properties of Palladium Nanoparticles Deposited on a Silanized Ceramic Membrane Support with a Flow-Through Method. *Industrial & Engineering Chemistry Research.* 2013;52(39):14099-14106.

21. Shekhah O, Wang H, Kowarik S, et al. Step-by-Step Route for the Synthesis of Metal-Organic Frameworks. *Journal of the American Chemical Society.* 2007;129(49):15118-15119.

22. Xu G-R, Wang S-H, Zhao H-L, et al. Layer-by-layer (LBL) assembly technology as promising strategy for tailoring pressure-driven desalination membranes. *Journal of Membrane Sci.* 2015;493:428-443.

23. Li Y, Zhou K, He M, Yao J. Synthesis of ZIF-8 and ZIF-67 using mixed-base and their dye adsorption. *Microporous and Mesoporous Materials.* 2016;234:287-292.

24. Fan X, Wang W, Li W, et al. Highly Porous ZIF-8 Nanocrystals Prepared by a

Surfactant Mediated Method in Aqueous Solution with Enhanced Adsorption Kinetics. *ACS Applied Materials & Interfaces*. 2014;6(17):14994-14999.